Fabrication of an Anisotropic Superhydrophobic Polymer Surface Using Compression Molding and Dip Coating

Kyong-Min Lee [1], Chi-Vinh Ngo [1], Ji-Young Jeong [2], Eun-chae Jeon [2], Tae-Jin Je [2] and Doo-Man Chun [1],* iD

[1] School of Mechanical Engineering, University of Ulsan, Ulsan 44610, Korea; qmfkdldjs907@hanmail.net (K.-M.L.); ngochivinh@gmail.com (C.-V.N.)

[2] Department of Nano Manufacturing Technology, Korea Institute of Machinery and Materials, Daejeon 34103, Korea; nano-jeong@kimm.re.kr (J.-Y.J.); jeonec@kimm.re.kr (E.-c.J.); jtj@kimm.re.kr (T.-J.J.)

* Correspondence: dmchun@ulsan.ac.kr; Tel.: +82-52-259-2706

Abstract: Many studies of anisotropic wetting surfaces with directional structures inspired from rice leaves, bamboo leaves, and butterfly wings have been carried out because of their unique liquid shape control and transportation. In this study, a precision mechanical cutting process, ultra-precision machining using a single crystal diamond tool, was used to fabricate a mold with microscale directional patterns of triangular cross-sectional shape for good moldability, and the patterns were duplicated on a flat thermoplastic polymer plate by compression molding for the mass production of an anisotropic wetting polymer surface. Anisotropic wetting was observed only with microscale patterns, but the sliding of water could not be achieved because of the pinning effect of the micro-structure. Therefore, an additional dip coating process with 1H, 1H, 2H, 2H-perfluorodecythricholosilanes, and TiO_2 nanoparticles was applied for a small sliding angle with nanoscale patterns and a low surface energy. The anisotropic superhydrophobic surface was fabricated and the surface morphology and anisotropic wetting behaviors were investigated. The suggested fabrication method can be used to mass produce an anisotropic superhydrophobic polymer surface, demonstrating the feasibility of liquid shape control and transportation.

Keywords: anisotropic superhydrophobic surface; hierarchical micro-nano structure; dip coating; compression molding; ultra-precision machining

1. Introduction

A superhydrophobic surface is defined as having a water droplet apparent contact angle above 150° and a sliding angle (SA) of less than 10° [1–3]. Superhydrophobic surfaces have unique characteristics, such as self-cleaning, anti-icing, anti-bio-adhesion, oil-water separation, water collection, drag reduction, and liquid droplet control. Superhydrophobic surfaces have been observed in nature including lotus leaves, tulip poplar leaves, rice leaves, and butterfly wings [1–6]. Among them, lotus leaves are typical isotropic superhydrophobic surfaces which can clean dust on the leaves by easy rolling of water droplets along all directions. Many artificial isotropic superhydrophobic surfaces inspired by nature have been fabricated by making nano or microscale surface patterns and low surface energy material coatings using various different fabrication methods, such as lithography, templating, chemical deposition, laser surface texturing, and nanoparticle coating [4–12]. In nature, rice leaves and butterfly wings have special anisotropic wettability and the water droplet can be easily moved along a certain direction, such as the direction parallel to the leaf edge in rice leaves or the radial

outward direction of the body's central axis in butterfly wings. This anisotropic superhydrophobic surface is important for liquid transport and liquid interactions on the surface for specific functionality such as self-cleaning of dust on a rice leaf and the prevention of water contact on the butterfly body [1,13]. This anisotropic wetting property can be realized mainly using structural patterned surfaces with nano or microscale parallel lines or grooves. Surfaces with line or groove patterns show two different wettabilities in the directions parallel and perpendicular to the pattern direction. As a result, the apparent contact angle and SA need to be measured along the two different directions and water droplet distortion using the ratio between the water droplet contact lengths according to two different directions has sometimes been observed. In addition, the contact angle hysteresis and wetting transition on anisotropic superhydrophobic surfaces shows unique behaviors according to the directions, and they are clearly different from the behaviors in isotropic wetting surfaces [14–17]. The lines or grooves have been fabricated by lithography, embossing, imprinting, laser machining, the formation of wrinkles via mechanical compressing, or other fabrication methods [13,18–28]. For mass production of an anisotropic wetting surface, replication of patterns using a mold seems to be suitable, but many studies have used poly(methyl methacrylate) (PDMS), which has a relatively long curing time and limited reusability of the mold [13,18–21], and molds with an uncontrollable surface roughness and side wall slope by laser machining and wrinkle formation, which does not show a clear pattern shape [7–11,13]. Additionally, the high surface energy ink pattern printing method can create various anisotropic superhydrophobic surfaces with low cost and large scale production especially 2D paper based applications [29]. However, the fabrication of anisotropic superhydrophobic surfaces on 3D polymer products is not easy with this method. Therefore, thermoplastic polymers for fast replication and precise pattern structures for better control of the anisotropic wettability effect are necessary for the mass production of an anisotropic superhydrophobic surface.

In this study, a precision mechanical cutting process, ultra-precision machining using a single crystal diamond tool, was used to fabricate a mold with microscale parallel groove patterns with a precise triangular shape. The patterns were duplicated on a flat polymer plate by compression molding for mass production of an anisotropic wetting polymer surface. Firstly, anisotropic wetting behavior was observed only with microscale patterns where the apparent contact angle parallel to the microscale pattern direction was higher than 150°. However, a low SA of the water droplet could not be achieved for water transport because of the pinning effect of the micro-structure. Therefore, additional dip coating with 1H, 1H, 2H, 2H-perfluorodecythricholosilanes, and TiO_2 nanoparticles was applied for a small sliding angle of a water droplet by non-directional nanoscale structure formation and low surface energy. As a result, an anisotropic superhydrophobic surface with a small SA was achieved. In addition, the surface morphology and anisotropic wetting behaviors were investigated with/without dip coating.

2. Materials and Methods

The groove patterns of the mold were designed with a microscale triangular cross-sectional shape for good moldability. In order to achieve precise pattern machining, an ultra-precision machining system (UVM-450C, Toshiba Co. Ltd., Tokyo, Japan) was used for the fabrication of the groove patterns on an electroplated copper mold with three different depths of 10, 20, and 30 μm and three different pitches of 20, 40, and 60 μm, respectively, as shown in Figure 1. The single crystal diamond tool has a 90° angle and the pitch was double the depth. The machining conditions are summarized in Table 1. After the fabrication of the groove patterns, the mold was cleaned with ethanol using an ultrasonic cleaner for 2 min. Then, the fabricated mold with microscale groove patterns was used for compression molding and pattern replication. For compression molding, a heating press (DIP-25J, Dae Heung Science Co. Ltd., Incheon, Korea) was used with a process pressure of 1 MPa and a process temperature of 180 °C for 5 min. A polypropylene (PP) plate (Quadrant Polypenco Co. Ltd., Cheonan, Korea) with a 5 mm thickness was used as the substrate material. After fabrication of the polymer surface with microscale groove patterns, the apparent contact angle and SA of five samples

were evaluated utilizing a contact angle meter (SmartDrop, Femtofab Co. Ltd., Seongnam, Korea) using deionized water droplets with a volume of 10 μL and a tilting speed of 1.6°/s for the SA. The surface morphology was observed using a confocal microscope (VK-X200 series, Keyence, Osaka, Japan) and a scanning electron microscope (SEM, JSM-7600F, JEOL, Tokyo, Japan). In order to provide a low surface energy on a polymer surface with nanoscale structures, the polymer surface with microscale groove patterns was coated by dip coating with silanization using ethanol, silane (1H, 1H, 2H, 2H-perfluorodecyltrichlorosilane), and the commercially-available anatase TiO_2 nanoparticles (5430MR, Nanostructured and Amorphous Materials Inc., Houston, TX, USA) with average particle size of 15 nm and the 99% purity at a mass ratio of 99:0.5:0.5 wt %, respectively [30–35]. The sample preparation procedures are summarized in Figure 2.
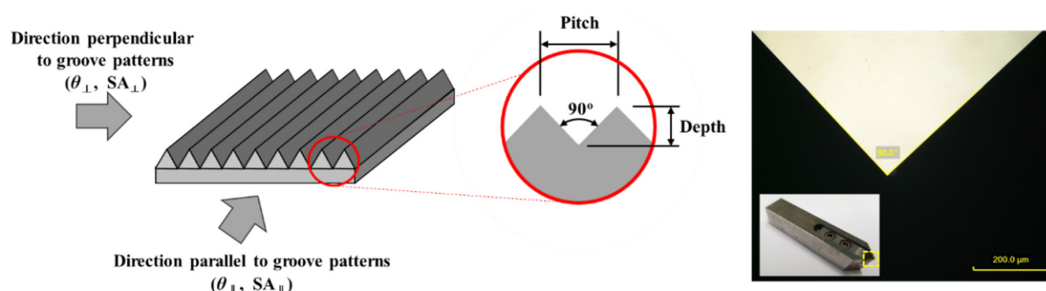
Figure 1. Design of the groove patterns and the images of the single crystal diamond tool and its tip.

Table 1. Machining conditions for the fabrication of the groove patterns.

Items	Conditions
Cutting tool	90° Single crystal diamond tool
Workpiece	Electroplated copper mold
Cutting depth	10 μm, 20 μm, 30 μm (Rough machining 5 μm × N, Semi-finishing 3 μm, and finishing 2 μm)
Pitch	20 μm, 40 μm, 60 μm
Feed rate	12,000 mm/min
Cutting oil	Isoparaffinic hydrocarbon solvent (ISOPAR-H)
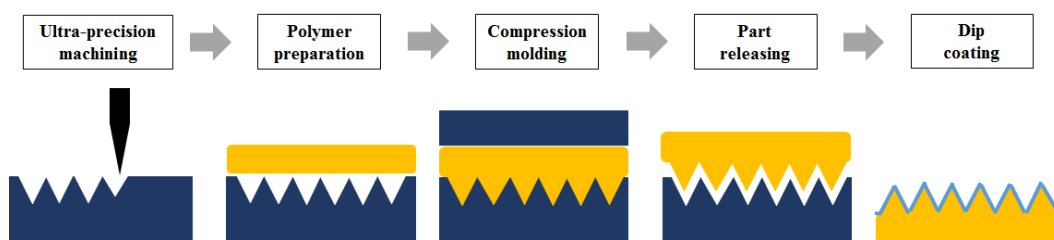
Figure 2. Schematic image of the fabrication procedure.

3. Results

3.1. Surface Morphology

The surface morphology of the mold fabricated by ultra-precision machining using a single crystal diamond tool was observed using a confocal microscope, as shown in Figure 3. Clear triangular grooves with three different depths of 10, 20, and 30 μm were obtained based on the design of the groove patterns. The surface morphology of the replicated PP surface also showed clear triangular grooves, as shown in Figure 4, and the measured average depths of five grooves were 10.6, 19.9, and 29.2 μm. Compression molding could successfully replicate the microscale structure. In addition, the surface roughness was slightly increased after dip coating, as shown in Figure 5. In order to evaluate the results of nanoparticle dip coating, the surface morphologies before and after dip coating were

compared using SEM, as shown in Figure 6. After dip coating, the agglomerated TiO$_2$ nanoparticles were randomly distributed on the mold surface.
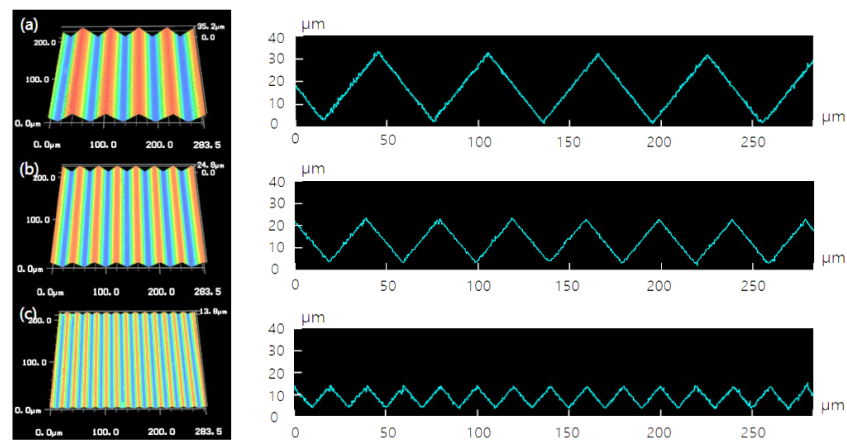

Figure 3. Confocal microscopy images of the fabricated pattern on the mold with (**a**) 10 μm, (**b**) 20 μm, and (**c**) 30 μm depths.
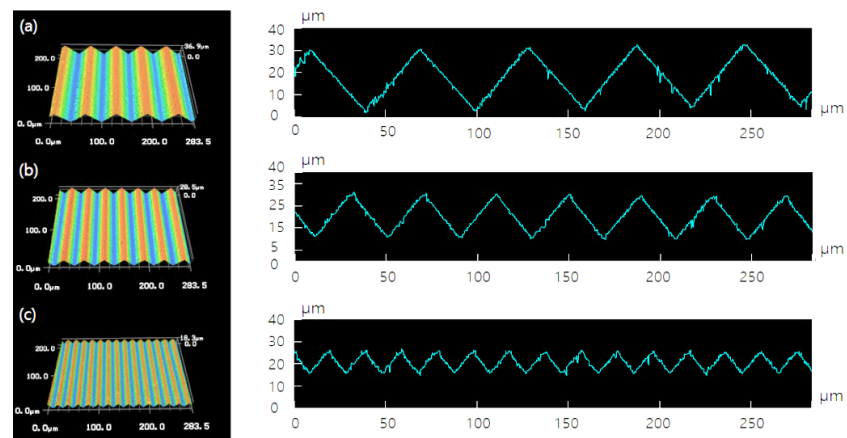

Figure 4. Confocal microscopy images of the replicated pattern on the polymer substrate with (**a**) 10 μm, (**b**) 20 μm, and (**c**) 30 μm depths.
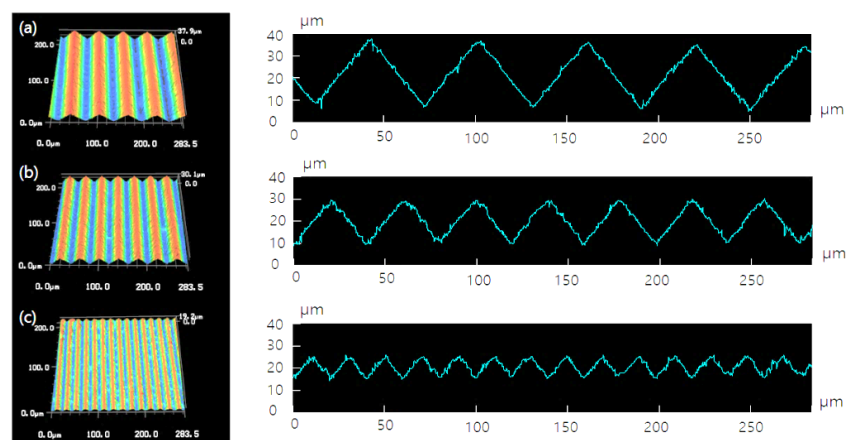

Figure 5. Confocal microscopy images of the dip-coated surface on the patterned polymer substrate with (**a**) 10 μm, (**b**) 20 μm, and (**c**) 30 μm depths.
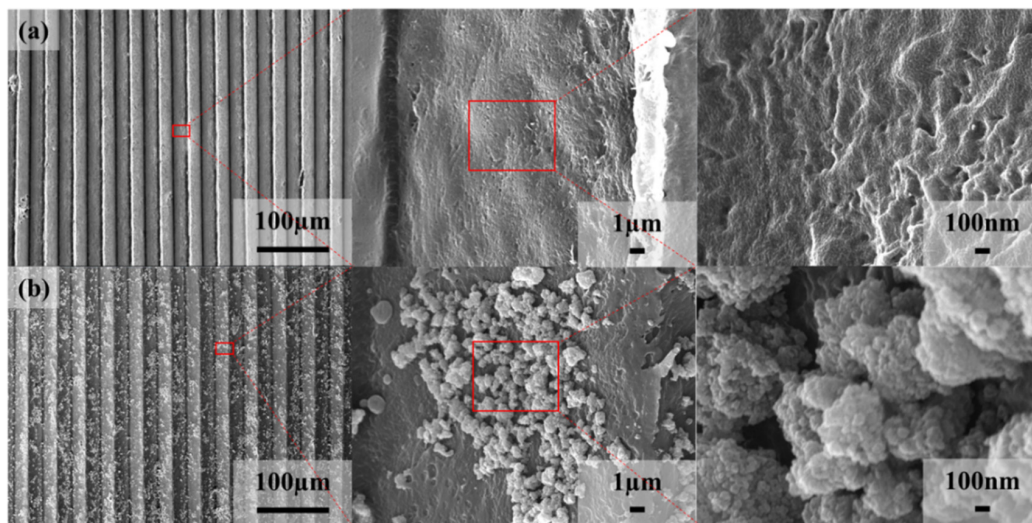
Figure 6. SEM images of the replicated surfaces: (**a**) before and (**b**) after dip coating.

3.2. Wettability

The wettability of the groove pattern surface has anisotropic behaviors and as a result, the apparent contact angle values in the directions parallel to the groove patterns ($\theta_{||}$) and the direction perpendicular to the groove patterns ($\theta_{\perp}$) were measured. The groove pattern surface without coating showed clear anisotropic wettability. The apparent contact angle on the flat PP surface without any groove patterns was 96° (hydrophobic) and all apparent contact angle values on the microscale groove pattern surface without coating were higher than the apparent contact angle value on the flat PP surface because of the increased roughness factor due to microscale grooves or air trapping in the grooves. Both apparent contact angles in the two different directions decreased as the groove depth increased and the apparent contact angle difference between the two different directions ($\Delta\theta$) increased as the groove depth increased, as shown in Figure 7. However, the sliding angles of the samples without coating could not be measured and the water droplet could not be moved even with a large tilting angle, even though the $\theta_{||}$ value with a groove depth of 10 µm was higher than 150° due to the strong pinning effect of microscale structures [24,36,37].
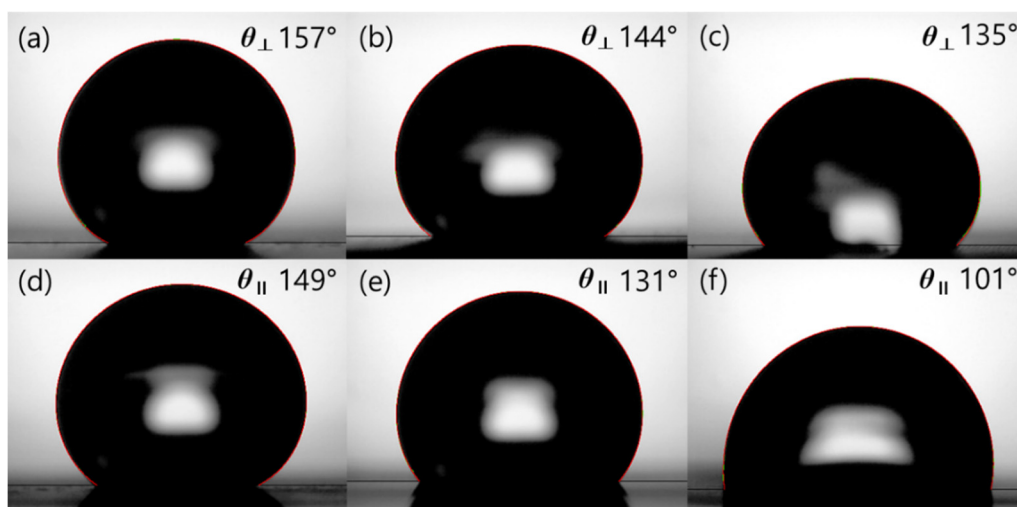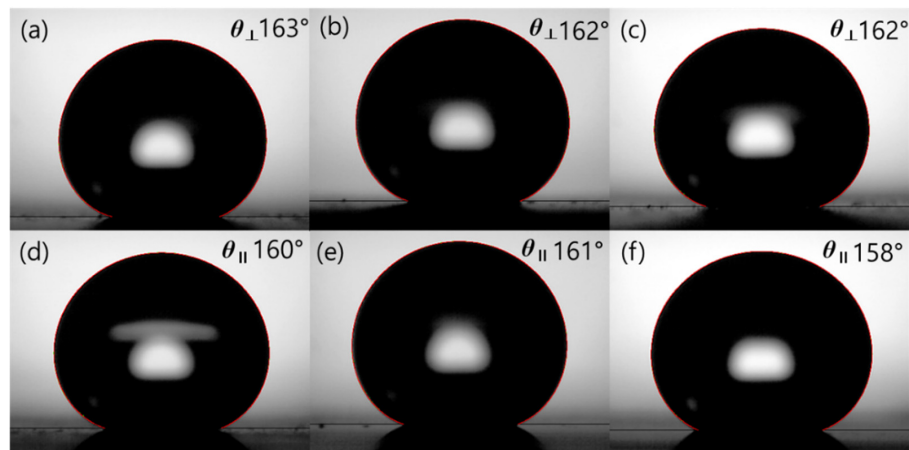

Figure 7. Water droplet contact angles on the microscale groove pattern surfaces without coating in the direction parallel to groove patterns with (**a**) 10 µm, (**b**) 20 µm, and (**c**) 30 µm depths, and in the direction perpendicular to the groove patterns with (**d**) 10 µm, (**e**) 20 µm, and (**f**) 30 µm depths.

After coating, the apparent contact angles in both directions were higher than 150° and the apparent contact angles did not show any clear differences. In addition, the $\theta_{\parallel}$ was slightly larger than $\theta_{\perp}$ with all of the different groove pattern surfaces, so that $\Delta\theta$ became very small (<5°), as shown in Figure 8. The reasons for these results are the low surface energy and the additional nanoscale structures due to dip coating. The coated surface on the flat PP plate had an apparent contact angle of 137°, which is much larger than the contact angle on the flat surface without coating (96°).

Figure 8. Water droplet contact angles on the microscale groove pattern surfaces with coating in the direction parallel to groove patterns with (**a**) 10 μm; (**b**) 20 μm; and (**c**) 30 μm depths, and in the direction perpendicular to the groove patterns with (**d**) 10 μm; (**e**) 20 μm; and (**f**) 30 μm depths.

After coating, all apparent contact angles were higher than 150° and $\Delta\theta$ was very small, demonstrating that the anisotropic wetting behavior became small. However, the SAs on the groove pattern surface with a coating showed clear anisotropic behaviors, as shown in Figure 9. The sliding angle in the parallel direction of the grove pattern ($SA_{\parallel}$) is smaller than the sliding angle in the perpendicular direction of the grove pattern ($SA_{\perp}$). Anisotropic small sliding could be clearly observed on the groove pattern surfaces with a 20 μm depth after coating (Video S1). Still, the microscale groove patterns affected the SAs even after coating and they resulted in anisotropic SAs. The water droplet could move along the microscale groove patterns more easily because of the lower $SA_{\parallel}$. This phenomenon is comparable to rice leaves [1,13].
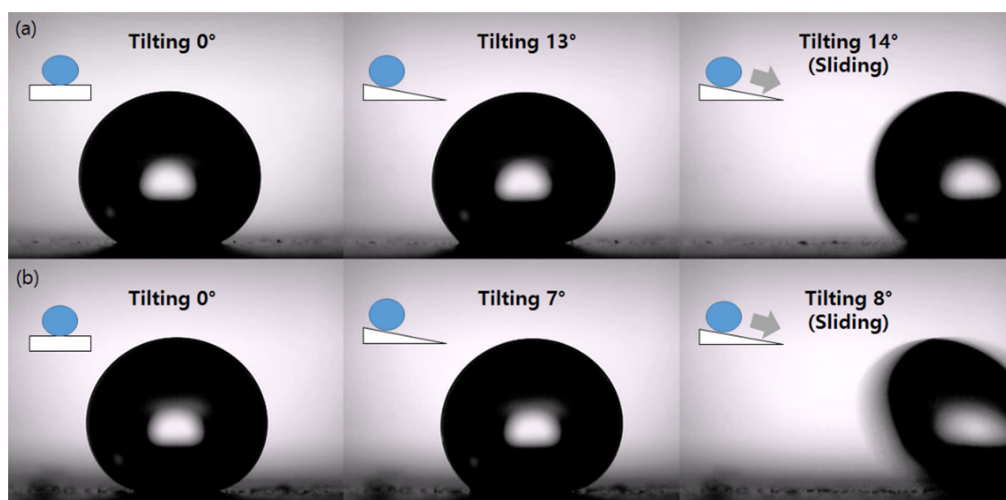

Figure 9. Sliding angles on the groove pattern surfaces with a 20 μm depth after coating in (**a**) the direction parallel to groove patterns; and (**b**) the direction perpendicular to the groove patterns.

The apparent contact angle and SA results on the groove patterns surfaces with/without coating are summarized in Figure 10. The error bars indicate the minimum and maximum values among five different samples. The anisotropic behavior of the apparent contact angle without coating depends on the microscale groove pattern depth, whereas anisotropic behavior of the apparent contact angle with coating was not clearly observed. After coating, the anisotropic behavior of the SA could be observed regardless of the groove pattern depth and the groove pattern surface with a 20 μm depth showed the lowest SAs.
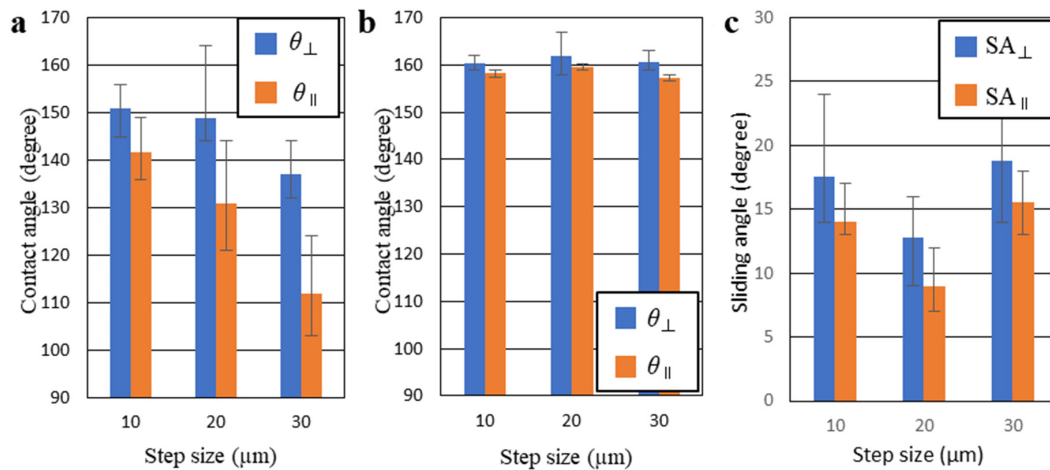
Figure 10. Summary of water droplet contact angles and sliding angles results: (**a**) the water droplet contact angles on the groove pattern surfaces without coating; (**b**) the water droplet contact angles; and (**c**) sliding angles on the groove pattern surfaces with coating.

The stability of the superhydrophobic coating is a very important issue. In order to evaluate the coating stability, the samples with the groove pattern surfaces with dip coating were stored in the ambient air for one year, and the apparent contact angle and sliding angle on the dip-coated samples were re-measured. Three samples for each pattern depth were used and the apparent contact angle and the sliding angle were measured three times for each sample. Figure 11 shows the result and the error bars indicate the maximum and minimum values. The apparent contact angle and the sliding angles did not show any clear changes, and this result confirmed the stability of the coating.
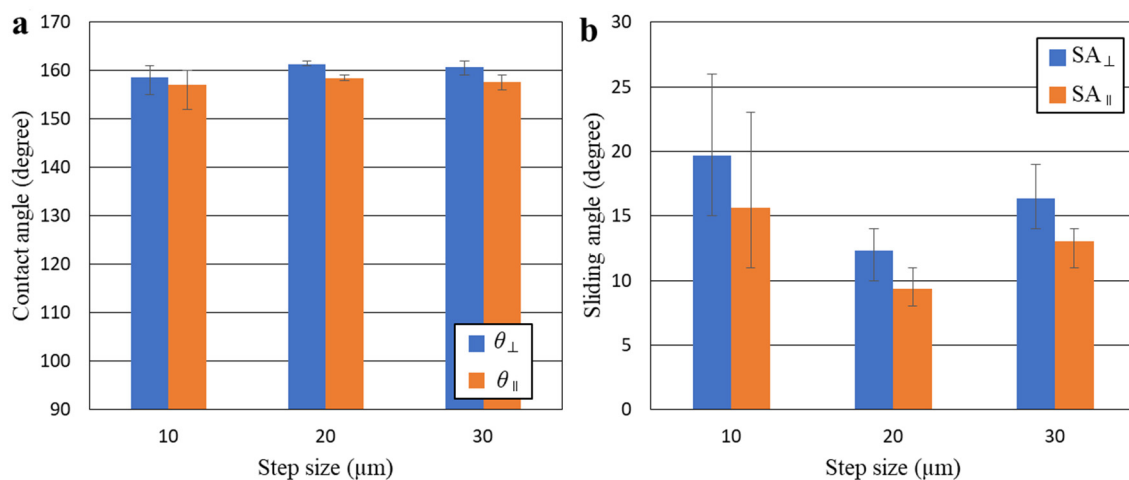

Figure 11. Apparent water droplet contact angles and sliding angles results after one year in ambient air: (**a**) the water droplet contact angles; and (**b**) sliding angles on the groove pattern surfaces with coating.

Contact angle hysteresis on the groove pattern surfaces with coating was evaluated using the tilting method with water droplet of 10 μL and tilting speed of 1.6°/s by the contact angle meter. The hysteresis was measured five times with one sample for each groove depth and the average values were summarized in the Table 2. As expected, the contact angle hysteresis on the direction parallel to groove patterns was smaller than the contact angle hysteresis on the direction perpendicular to groove patterns like the sliding angles. The contact angle hysteresis of the sample with 20 μm groove depth was the lowest. The differences of the receding and advancing contact angles between parallel and perpendicular directions showed less than 8°. It was reported that the receding contact angle and the advancing contact angle appeared isotropic with a small solid fraction on the superhydrophobic stripes and the cosine values of receding and advancing contact angle were in the region of less than 0.2 of solid fraction from the research of Dubov et al. [14]. The hysteresis results were in good agreement with the findings of Dubov et al. However, the geometry of patterns in this research was different from superhydrophobic strips, so the effect of geometry should be studied in the future work.

Table 2. Contact angle hysteresis results on the groove pattern surfaces with coating.

Groove Depth	Direction Parallel to Groove Patterns			Direction Perpendicular to the Groove Patterns		
	Advancing Contact Angle	Receding Contact Angle	Contact Angle Hysteresis	Advancing Contact Angle	Receding Contact Angle	Contact Angle Hysteresis
10 μm	159.9°	132.6°	27.2°	164.0°	127.8°	36.1°
20 μm	168.3°	154.1°	14.2°	174.2°	149.8°	24.4°
30 μm	167.2°	146.5°	20.7°	174.8°	140.8°	34.1°

4. Discussion

Isotropic wetting behaviors can be simply explained by two wetting models which were developed by Wenzel in 1936 [38] and Cassie–Baxter in 1944 [39]. The Wenzel model is used to describe the contact angle in a non-composite or full wetting state and the Cassie–Baxter model is used to describe the contact angle in a composite or partial wetting state. However, recent studies have found that Wenzel and Cassie–Baxter models are not suitable for predicting the contact angle on an anisotropic surface because of the pinning effect of surface patterns [24,36,37]. In addition, a water droplet on a micro-structured surface exhibits both the non-composite and composite states at the same time due to the microscale surface pattern orientation [24,40,41]. In this research, anisotropic wetting behaviors with microscale groove patterns without coating were clearly observed and the contact angle predicted by the Wenzel model is much smaller than the measured apparent contact angle. The Δθ value increased as the pitch and depth increased, and these results are comparable to the results of other studies [24,37].

After coating, the surface roughness increased due to newly-formed nano-structures, both $θ_{||}$ and $θ_⊥$ increased, Δθ decreased, and anisotropic sliding of a water droplet was achieved. These trends are in good agreement with the findings of Lee et al. and can be explained based on the surface roughness and surface free energy. A large contact angle hysteresis pins water droplets on the surface at a low surface roughness of a nanostructure, whereas a small anisotropic contact angle hysteresis generates directional movement of the water droplet, as observed on a rice leaf, and a water droplet on the surface with patterns tends to slide more easily along the direction parallel to the patterns due to the lower energy barrier for wetting [20]. In this research, the apparent contact angle on the flat surface with coating was 137°, which is much larger than the apparent contact angle (98°) on the flat surface without coating due to the low surface free energy by silanization and increased nanoscale surface roughness resulting from the TiO_2 nanoparticle coating.

After coating, the PP surface with microscale groove patterns showed apparent contact angles higher than 150°. The water droplet with small volumes could not be dispensed properly. The adhesion force from the nozzle of the water dispenser was stronger than the force from the coated and patterned PP surface with a small water droplet volume. The water droplet with an 8 μL volume could not

be dispensed on the patterned surface with coating even though the water droplet was squeezed by the nozzle, as shown in Figure 12a (Video S2). In addition, a water droplet was dropped from about a 3 cm height and bouncing of the water droplet on the 3°-tilted coated sample was observed without water droplet adhesion, as shown in Figure 12b (Video S3). Thus, the surfaces prepared by means of the method (compression molding and dip coating) discussed herein demonstrated simple sample preparation and good anisotropic superhydrophobic performances with a low SA. The results suggest that they could be applied favorably in various potential applications, including control of water adhesion and transfer of water droplets with mass production of an anisotropic superhydrophobic surface.
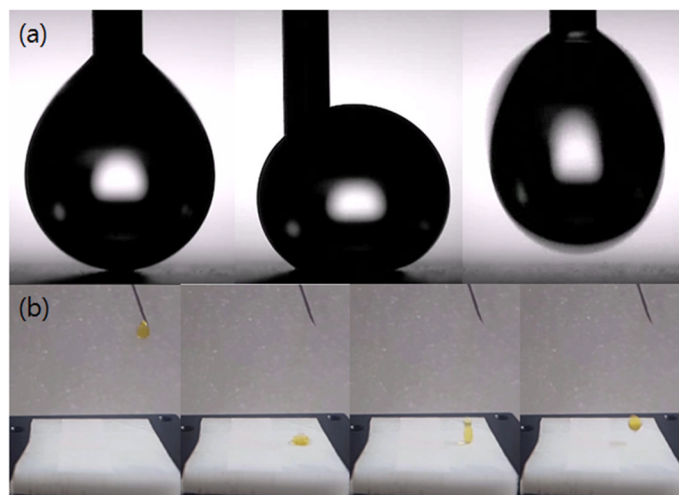
Figure 12. Demonstrations of the superhydrophobicity: (**a**) touching of an 8 μL water droplet onto a coated sample with 20 μm depth groove patterns; and (**b**) bouncing of a water droplet dropped from a 3 cm height.

The well-known superhydrophobic lotus leaves can be either hydrophobic or hydrophilic by water condensation on their surfaces [42]. In order to check the surface performance with condensed water, water condensation testing was carried out with the dip-coated sample with the 20 μm groove pattern depth three times. Water was condensed on the samples above a beaker of boiling water for 10 min. The condensed water remained on the samples even with 90° tilting. The condensed water droplets showed hydrophobic (not superhydrophobic) and they did not roll off the surface with tilting. This phenomenon was found from lotus leaves and the reason was that water droplets formed from the vapor phase can be trapped in the nanoscale structures on the surface, and the trapped water drops can remain trapped as they grow or become merged with larger drops [42]. Just after the condensed water droplets were blown by air without any additional drying or a long period of time, the apparent contact angles and sliding angles with the three dip-coated samples with a 20 μm groove pattern depth showed average apparent contact angles of 161° ($\theta_{||}$) and 163° ($\theta_{\perp}$) and average sliding angles of 9° ($SA_{||}$) and 13° ($SA_{\perp}$), the results were similar to the results before water condensation test. This result indicates that the condensed water can be trapped and showed sticky behavior by formation of water droplet in the nanoscale structures, but the superhydrophobicity can be easily recovered by removing the condensed water.

One of important issues in superhydrophobicity is the wetting transition from the Cassie-Baxter state to the Wenzel state according to time and an external pressure [43,44]. When the wetting state on the superhydrophobic surface is not stable, the remarkable contact angle change can be observed according to time and an external pressure. In Figure 12a (Video S2), the external pressure was applied to the water droplet by the nozzle, and it did not show a wetting transition. In addition, the apparent contact angle change was observed for 20 min. Every 5 min the apparent contact angle was measured,

and the apparent contact angle was slightly decreased. However, there was no remarkable contact angle change or the transition of wetting state. The slightly decreased apparent contact angle can be explained with the evaporation of water droplet and the receding contact angle from contact angle hysteresis. As shown in Figure 13, the volume of water droplet and the contact angles were slightly decreased according to time, but clear wetting transition could not be observed.
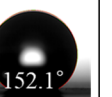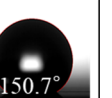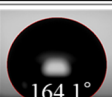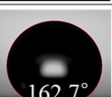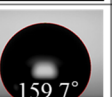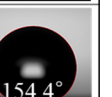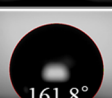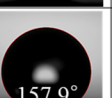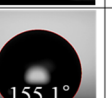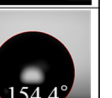
Dire-ction	Pattern depth	Time				
		0 min	5 min	10 min	15 min	20 min
Direction parallel to groove patterns	10 μm	160.9°	159.2°	158.2°	152.1°	152.1°
	20 μm	160.4°	159.8°	156.6°	154.7°	152.6°
	30 μm	158.3°	155.5°	152.9°	151.4°	150.7°
Direction perpendicular to groove patterns	10 μm	164.8°	161.3°	158.7°	157.2°	156.4°
	20 μm	164.1°	162.7°	159.7°	156.3°	154.4°
	30 μm	161.8°	158.1°	157.9°	155.1°	154.4°

Figure 13. The change of apparent contact angle on the groove pattern surfaces with coating according to a time of 20 min.

5. Conclusions

In this study, ultra-precision machining using a single crystal diamond tool was used to fabricate a mold with microscale directional groove patterns of triangular cross-sectional shape for good moldability and the patterns were duplicated on a flat thermoplastic polymer plate by compression molding for mass production of an anisotropic wetting polymer surface. Anisotropic apparent contact angles were observed only with microscale patterns, but sliding of water could not be achieved because of the pinning effect of the micro-structure. Therefore, an additional dip coating process with 1H, 1H, 2H, 2H-perfluorodecythricholosilanes, and TiO_2 nanoparticles was applied for a small sliding angle with nanoscale pattern and low surface energy. The anisotropic superhydrophobic surface was successfully fabricated where the resulting apparent contact angle was above 150° and the $SA_{||}$ was smaller than 10°. The suggested fabrication method can be used to mass produce an anisotropic superhydrophobic polymer surface, demonstrating the feasibility of anisotropic liquid shape control and liquid transportation.

References

1. Feng, L.; Li, S.; Li, Y.; Li, H.; Zhang, L.; Zhai, J.; Song, Y.; Liu, B.; Jiang, L.; Zhu, D. Super-hydrophobic surfaces: From natural to artificial. *Adv. Mater.* **2002**, *14*, 1857–1860. [CrossRef]

2. Ganesh, V.A.; Raut, H.K.; Nair, A.S.; Ramakrishna, S. A review on self-cleaning coatings. *J. Mater. Chem.* **2011**, *21*, 16304–16322. [CrossRef]

3. Sas, I.; Gorga, R.E.; Joines, J.A.; Thoney, K.A. Literature review on superhydrophobic self-cleaning surfaces produced by electrospinning. *J. Polym. Sci. Polym. Phys.* **2012**, *50*, 824–845. [CrossRef]

4. Yan, Y.Y.; Gao, N.; Barthlott, W. Mimicking natural superhydrophobic surfaces and grasping the wetting process: A review on recent progress in preparing superhydrophobic surfaces. *Adv. Colloid Interface Sci.* **2011**, *169*, 80–105. [CrossRef] [PubMed]

5. Malshe, A.; Rajurkar, K.; Samant, A.; Hansen, H.N.; Bapat, S.; Jiang, W. Bio-inspired functional surfaces for advanced applications. *CIRP Ann. Manuf. Technol.* **2013**, *62*, 607–628. [CrossRef]

6. Darmanin, T.; Guittard, F. Recent advances in the potential applications of bioinspired superhydrophobic materials. *J. Mater. Chem. A* **2014**, *2*, 16319–16359. [CrossRef]

7. Davaasuren, G.; Ngo, C.; Oh, H.; Chun, D.M. Geometric study of transparent superhydrophobic surfaces of molded and grid patterned polydimethylsiloxane (PDMS). *Appl. Surf. Sci.* **2014**, *314*, 530–536. [CrossRef]

8. Chun, D.M.; Davaasuren, G.; Ngo, C.; Kim, C.; Lee, G.; Ahn, S. Fabrication of transparent superhydrophobic surface on thermoplastic polymer using laser beam machining and compression molding for mass production. *CIRP Ann. Manuf. Technol.* **2014**, *63*, 525–528. [CrossRef]

9. Ngo, C.; Davaasuren, G.; Oh, H.; Chun, D.M. Transparency and superhydrophobicity of cone-shaped micropillar array textured polydimethylsiloxane. *Int. J. Precis. Eng. Manuf.* **2015**, *16*, 1347–1353. [CrossRef]

10. Simpson, J.T.; Hunter, S.R.; Aytug, T. Superhydrophobic materials and coatings: A review. *Rep. Prog. Phys.* **2015**, *78*, 086501. [CrossRef] [PubMed]

11. Chun, D.M.; Ngo, C.; Lee, K. Fast fabrication of superhydrophobic metallic surface using nanosecond laser texturing and low-temperature annealing. *CIRP Ann. Manuf. Technol.* **2016**, *65*, 519–522. [CrossRef]

12. Ngo, C.V.; Chun, D.M. Laser Printing of Superhydrophobic Patterns from Mixtures of Hydrophobic Silica Nanoparticles and Toner Powder. *Sci. Rep.* **2016**, *6*, 36735. [CrossRef] [PubMed]

13. Xia, D.; Johnson, L.M.; López, G.P. Anisotropic wetting surfaces with one-dimesional and directional structures: Fabrication approaches, wetting properties and potential applications. *Adv. Mater.* **2012**, *24*, 1287–1302. [CrossRef] [PubMed]

14. Dubov, A.L.; Mourran, A.; Möller, M.; Vinogradova, O.I. Contact angle hysteresis on superhydrophobic stripes. *J. Chem. Phys.* **2014**, *141*, 074710. [CrossRef] [PubMed]

15. Dubov, A.L.; Mourran, A.; Möller, M.; Vinogradova, O.I. Regimes of wetting transitions on superhydrophobic textures conditioned by energy of receding contact lines. *Appl. Phys. Lett.* **2015**, *106*, 241601. [CrossRef]

16. Kavousanakis, M.E.; Colosqui, C.E.; Papathanasiou, A.G. Engineering the geometry of stripe-patterned surfaces towards efficient wettability switching. *Colloid Surf. A* **2013**, *436*, 309–317. [CrossRef]

17. Bormashenko, E. Comment on water droplet motion control on superhydrophobic surfaces: Exploiting the Wenzel-to-Cassie transition. *Langmuir* **2011**, *27*, 12769–12770. [CrossRef] [PubMed]

18. Wu, D.; Wang, J.; Wu, S.; Chen, Q.; Zhao, S.; Zhang, H.; Sun, H.; Jiang, L. Three-level biomimetic rice-leaf surfaces with controllable anisotropic sliding. *Adv. Funct. Mater.* **2011**, *21*, 2927–2932. [CrossRef]

19. Kang, S.M.; Lee, C.; Kim, H.N.; Lee, B.J.; Lee, J.E.; Kwak, M.K.; Suh, K. Directional oil sliding surfaces with hierarchical anisotropic groove microstructures. *Adv. Mater.* **2013**, *25*, 5756–5761. [CrossRef] [PubMed]

20. Lee, S.G.; Lim, H.S.; Lee, D.Y.; Kwak, D.; Cho, K. Tunable anisotropic wettability of rice leaf-like wavy surfaces. *Adv. Funct. Mater.* **2013**, *23*, 547–553. [CrossRef]

21. Wang, S.; Yu, N.; Wang, T.; Ge, P.; Ye, S.; Xue, P.; Liu, W.; Shen, H.; Zhang, J.; Yang, B. Morphology-patterned anisotropic wetting surface for fluid control and gas–liquid separation in microfluidics. *ACS Appl. Mater. Interface* **2016**, *8*, 13094–13103. [CrossRef] [PubMed]

22. Zhao, Y.; Lu, Q.; Li, M.; Li, X. Anisotropic wetting characteristics on submicrometer-scale periodic grooved surface. *Langmuir* **2007**, *23*, 6212–6217. [CrossRef] [PubMed]

23. Li, W.; Fang, G.; Li, Y.; Qiao, G. Anisotropic wetting behavior arising from superhydrophobic surfaces: Parallel grooved structure. *J. Phys. Chem. B* **2008**, *112*, 7234–7243. [CrossRef] [PubMed]

24. Li, P.; Xie, J.; Cheng, J.; Wu, K. Anisotropic wetting properties on a precision-ground micro-V-grooved Si surface related to their micro-characterized variables. *J. Micromech. Microeng.* **2014**, *24*, 075004. [CrossRef]

25. Liang, Y.; Shu, L.; Natsu, W.; He, F. Anisotropic wetting characteristics versus roughness on machined surfaces of hydrophilic and hydrophobic materials. *Appl. Surf. Sci.* **2015**, *331*, 41–49. [CrossRef]

26. Tie, L.; Guo, Z.; Liu, W. Anisotropic wetting properties on various shape of parallel grooved microstructure. *J. Colloid Interface Sci.* **2015**, *453*, 142–150. [CrossRef] [PubMed]

27. Tang, Y.; Xu, X.; Hou, G.; Huazhen, C.; Guoqu, Z. Facile approach to prepare a quasi-one-dimensional anisotropic wetting surface on copper substrate and its wetting properties. *RSC Adv.* **2015**, *5*, 64749–64755. [CrossRef]

28. Asakura, K.; Yan, J. Water repellency control of oxygen-free copper surface by diamond-cut micro grooves. *Int. J. Automot. Technol.* **2015**, *9*, 396–402. [CrossRef]

29. Balu, B.; Berry, A.D.; Patel, K.T.; Breedveld, V.; Hess, D.W. Directional Mobility and Adhesion of Water Drops on Patterned Superhydrophobic Surfaces. *J. Adhes. Sci. Technol.* **2011**, *25*, 627–642. [CrossRef]

30. Contreras, C.B.; Chagas, G.; Strumia, M.C.; Weibel, D.E. Permanent superhydrophobic polypropylene nanocomposite coatings by a simple one-step dipping process. *Appl. Surf. Sci.* **2014**, *307*, 234–240. [CrossRef]

31. Wang, G.; Liu, S.; Wei, S.; Liu, Y.; Lian, J.; Jiang, Q. Robust superhydrophobic surface on Al substrate with durability, corrosion resistance and ice-phobicity. *Sci. Rep.* **2016**, *6*, 20933. [CrossRef] [PubMed]

32. Gao, L.; Lu, Y.; Zhan, X.; Li, J.; Sun, Q. A robust, anti-acid, and high-temperature–humidity-resistant superhydrophobic surface of wood based on a modified TiO_2 film by fluoroalkyl silane. *Surf. Coat. Technol.* **2015**, *262*, 33–39. [CrossRef]

33. Li, S.; Jin, M.; Yu, C.; Liao, M. Wetting behavior of superhydrophobic surface in the liquid influenced by the existing of air layer. *Colloids Surf. Physicochem. Eng. Asp.* **2013**, *430*, 46–50. [CrossRef]

34. Ramanathan, R.; Weibel, D.E. Novel liquid–solid adhesion superhydrophobic surface fabricated using titanium dioxide and trimethoxypropyl silane. *Appl. Surf. Sci.* **2012**, *258*, 7950–7955. [CrossRef]

35. Bernagozzi, I.; Antonini, C.; Villa, F.; Marengo, M. Fabricating superhydrophobic aluminum: An optimized one-step wet synthesis using fluoroalkyl silane. *Colloids Surf. Physicochem. Eng. Asp.* **2014**, *441*, 919–924. [CrossRef]

36. Chen, Y.; He, B.; Lee, J.; Patankar, N.A. Anisotropy in the wetting of rough surfaces. *J. Colloid Interface Sci.* **2005**, *281*, 458–464. [CrossRef] [PubMed]

37. Yang, J.; Rose, F.R.; Gadegaard, N.; Alexander, M.R. Effect of sessile drop volume on the wetting anisotropy observed on grooved surfaces. *Langmuir* **2009**, *25*, 2567–2571. [CrossRef] [PubMed]

38. Wenzel, R.N. Resistance of solid surfaces to wetting by water. *Ind. Eng. Chem.* **1936**, *28*, 988–994. [CrossRef]

39. Cassie, A.; Baxter, S. Wettability of porous surfaces. *Trans. Faraday Soc.* **1944**, *40*, 546–551. [CrossRef]

40. Kong, L.; Cheung, C.; To, S.; Cheng, C. Modeling and characterization of generation of 3D micro-structured surfaces with self-cleaning and optical functions. *Optik Int. J. Light Electron Opt.* **2013**, *124*, 2848–2853. [CrossRef]

41. Feng, L.; Zhang, Y.; Xi, J.; Zhu, Y.; Wang, N.; Xia, F.; Jiang, L. Petal effect: A superhydrophobic state with high adhesive force. *Langmuir* **2008**, *24*, 4114–4119. [CrossRef] [PubMed]

42. Cheng, Y.T.; Rodak, D.E. Is the lotus leaf superhydrophobic? *Appl. Phys. Lett.* **2005**, *86*, 144101. [CrossRef]

43. Aslanidou, D.; Karapanagiotis, I.; Panayiotou, C. Tuning the wetting properties of siloxane-nanoparticle coatings to induce superhydrophobicity and superoleophobicity for stone protection. *Mater. Des.* **2016**, *108*, 736–744. [CrossRef]

44. Yao, X.; Chen, Q.; Xu, L.; Li, Q.; Song, Y.; Gao, X.; Quéré, D.; Jiang, L. Bioinspired ribbed nanoneedles with robust superhydrophobicity. *Adv. Funct. Mater.* **2010**, *20*, 656–662. [CrossRef]